Smart Materials and Structures

PAPER • **OPEN ACCESS**

The investigation of the energy harvesting performance using electrospun PTFE/PVDF based on a triboelectric assembly

To cite this article: Pattarinee White *et al* 2024 *Smart Mater. Struct.* **33** 075010

OPEN ACCESS
IOP Publishing
Smart Materials and Structures
Smart Mater. Struct. **33** (2024) 075010 (12pp)
https://doi.org/10.1088/1361-665X/ad508d

The investigation of the energy harvesting performance using electrospun PTFE/PVDF based on a triboelectric assembly

Pattarinee White[1,2,*], Piyapong Pankaew[3], Dmitry Bavykin[4], M Moshrefi-Torbati[5] and Stephen Beeby[1]

[1] Centre for Flexible Electronics and E-Textiles, University of Southampton, Southampton, United Kingdom
[2] Division of Physics, Rajamangala University of Technology Krungthep, Bangkok, Thailand
[3] Division of Industrial Materials Science, Rajamangala University of Technology Phra Nakhon, Bangkok, Thailand
[4] Energy Technology Group, University of Southampton, Southampton, United Kingdom
[5] Mechatronics Research Group, University of Southampton, Southampton, United Kingdom

E-mail: p.white@soton.ac.uk, piyapong.p@rmutp.ac.th, d.bavykin@soton.ac.uk, m.m.torbati@soton.ac.uk and spb@ecs.soton.ac.uk

Received 1 April 2024, revised 3 May 2024
Accepted for publication 24 May 2024
Published 6 June 2024

Abstract

This work presents an investigation into the energy harvesting performance of a combination of polytetrafluoroethylene (PTFE) and polyvinylidene fluoride (PVDF) materials prepared using a one-step electrospinning technique. Before electrospinning, different percentages of the 1 micron PTFE powder were added to a PVDF precursor. The surface morphology of the electrospun PTFE/PVDF fibre was investigated using a scanning electron microscope and tunnelling electron microscope. The structure was investigated using Fourier-transform infrared spectroscopy and x-ray diffraction analysis (XRD). A highly porous structure was observed with a mix of the α- and β-phase PVDF. The amount of β-phase was found to reduce when increasing the percentage of PTFE. The maximum amount of PTFE that could be added and still be successfully electrospun was 20%. This percentage showed the highest energy harvesting performance of the different PTFE/PVDF combinations. Electrospun fibres with different percentages of PTFE were deployed in a triboelectric energy harvester operating in the contact separation mode and the open circuit voltage and short circuit current were obtained at frequencies of 4–9 Hz. The 20% PTFE fibre showed 4 (51–202 V) and 7 times (1.3–9.04 μA) the voltage and current output respectively when compared with the 100% PVDF fibre. The V_{oc} and I_{sc} were measured for different load resistances from 1 kΩ to 6 GΩ and achieved a maximum power density of 348.5 mW m^{-2} with a 10 MΩ resistance. The energy stored in capacitors 0.1, 0.47, 1, and 10 μF from a book shaped PTFE/PVDF energy harvester were 1.0, 16.7, 41.2 and 136.8 μJ, respectively. The electrospun fibre is compatible with wearable and e-textile applications as it is breathable and flexible. The electrospun PTFE/PVDF was assembled into shoe insoles to demonstrate energy harvesting performance in a practical application.

* Author to whom any correspondence should be addressed.

Supplementary material for this article is available online

Keywords: textile triboelectric nanogenerator, wearable devices, electrospinning, PTFE, PVDF

1. Introduction

From 2023 to 2030, the market for wearable smart technology is predicted to grow by 14.6% [1]. A rapidly developing platform for wearable technology is electronic textiles (e-textiles or smart fabrics). E-textile manufacturing technologies enable wearables to be integrated within garments providing a comfortable and familiar platform. The use of conventional rigid batteries is incompatible with such platforms, and these also need to be regularly charged and replaced and are environmentally harmful [2, 3]. Therefore alternative textile compatible energy harvesting and self-powered sensing technologies powered by ambient energy sources are of considerable interest [4]. The ability to transform human motion-based mechanical energy into electrical energy has been demonstrated utilising piezoelectric materials [5–7] electromagnetic devices [8], electrostatic mechanisms (via the electret/ferroelectret [9, 10] and triboelectric effects [11–13]), and electroactive polymers [14–16] transduction mechanisms.

The triboelectric effect, whereby electrical energy is generated from the triboelectrification of materials during cyclical physical contact [17], has been exploited in many example energy harvesting devices [18]. The first a triboelectric nanogenerator (TENG) demonstrated the potential of electrostatic charge transfer in energy harvesting technologies [19]. Textiles are attractive materials for realising TENGs due to their affinity to gain or lose ions during contact and many examples have been demonstrated [20–22]. Novel textile TENGs have also been used in self-powered biomonitoring applications, for example, in wearable cardiovascular and respiratory monitoring [23].

The approaches to enhance the contact-electrification within TENGs and therefore increase the electrical output typically involve three basic methods: modifying surface morphology, modifying surface chemistry, and utilising ferroelectric materials [24]. There are various mechanisms by which the use or addition of ferroelectric materials can improve triboelectrification. Early theories based upon the change in work function of the ferroelectric polymer which enhances electron transfer [25] have been superseded by research that demonstrates it is due to the piezoelectric effect whereby charge is generated within the material during contact that increase electrostatic induction [26]. Polyvinylidene fluoride (PVDF) is one such ferroelectric polymer commonly used in TENGs [27–30]. Electrospun PVDF fibres have demonstrated effective energy conversion when used as the negative triboelectric material [31–33] and the electrical output of PVDF fibres has been further increased by the addition of other fibrous materials within the generator. For example, the combination of PVDF and polyamide 6 fibres produces a 25% increase in peak voltage compared with PVDF fibres alone [34]. Electrospun fibres are inherently compatible with textiles being virtually identical in nature to the fibres used in yarns or non-woven fabrics. Electrospun fibre mats possess the desirable characteristics associated with textiles of breathability, flexibility and feel. Electrospun functional fibres have been used to create smart textiles with advanced functionality. For example, electrospun PVDF nanofibre membranes have been evaluated in face masks and shown to significantly improve the filtration efficiency [35].

Polytetrafluoroethylene (PTFE) has amongst the strongest electron affinity amongst the triboelectric materials placing it at the negative end of the triboelectric series [34, 36]. It is also an excellent electret material being a dielectric material able to quasi-permanently trap surface charge typically generated by ion irradiation [37]. Thus, many TENGs have been demonstrated with PTFE as a negative material [13, 38, 39]. Typically, the PTFE is obtained from commercial sources and the energy harvesting performance is influenced by the manufacturing process. Electrospinning techniques can be used to improve the triboelectric properties by modifying the surface morphology and increasing the surface area of the material. Additionally, during the electrospinning process, a high voltage is applied to the polymer solution which results in a high volume of charged particles being introduced into the solution, which are subsequently trapped within the electrospun fibre after solidification. However, fabricating PTFE using electrospinning is challenging due to its extremely stable chemical and thermal properties making it extremely difficult to obtain a solution suitable for electrospinning without chemical modification [40]. Zhao *et al* investigated energy harvesting from electrospun PTFE fibres by utilising polyethene oxide (PEO) water solution as a carrier [41]. Here the precursor polymer solution was employed to create a PTFE/PEO structure using emulsion electrospinning. A sintering step at over 350 °C is required to remove the carrier leaving PTFE nanofibres.

This paper presents an evaluation of the energy harvesting performance of an electrospun PTFE/PVDF composite TENG. This combination exploits the extremely strong negative affinity of the PTFE with the piezoelectric charge generation properties of the PVDF ferroelectric polymer. The work builds upon a preliminary study [42] that investigated composite materials up to 4% PTFE. Here the systematic evaluation of the percentage of PTFE in the PVDF fibre is presented and the PTFE 20%/PVDF 80% composite fibre achieved a 4 times increase in open circuit voltage (51–202 V) and a 7 times increase in short circuit current (1.3–9.04 μA) when compared with the 100% PVDF fibre. The paper also presents the application of the electrospun PTFE/PVDF fibre mat combined with a nylon fabric in a shoe insole where the composite material again produces a significant increase in

the power output when compared with a pure PVDF fibre mat.

2. Experimental section

2.1. Electrospun fibre preparation

The fabrication of the electrospun PTFE/PVDF fibres is illustrated in figure 1. PVDF (Sigma Aldrich, Dorset, UK, Mw = 534 000) and PTFE (Sigma Aldrich, 1 mm mean diameter particles) powders were blended together in the following ratios: PTFE1% + PVDF 19%, PTFE2% + PVDF 18%, PTFE3% + PVDF 17%, PTFE4% + PVDF 16%, PTFE5% + PVDF 15%, PTFE6% + PVDF 14%, and PTFE7% + PVDF 13%. Each PTFE/PVDF powder blend was then combined with a solvent solution of N-Dimethylformamide (DMF, Sigma Aldrich, Dorset, UK, 99.8%) and acetone (Fisher Scientific, Waltham, MA, USA, 99.6%) mixed in a 7:3 ratio. The solvent solution was stirred at 60 °C using a magnetic hotplate stirrer for a total of six hours before adding the powder blend at a ratio of 20% powder 80% solvent by weight. To prevent the PTFE particles from agglomerating, the solution was sonicated for six hours prior to mixing with the PVDF and DMF: acetone solvent [43].

The PTFE/PVDF solution was put in a 3 ml syringe with a blunt tip (21 G) needle and attached to the syringe pump of the electrospinning apparatus (EC-DIC, IME Technologies, Netherlands). For each concentration, the distance between the tip and the substrate, the applied voltage, the flow rate, and the rotational speed of the drum remained constant at 22 cm, 25 kV, 2 ml hr^{-1}, and 150 rpm, respectively. The PTFE/PVDF fibre was collected as a nonwoven fibre mat and assembled into a triboelectric energy harvester without any additional processing.

2.2. Fibre characterisation

After electrospinning, the solvent was fully evaporated, and it can be assumed that the percentages of PTFE in the solid fibre are as stated in table 2. The morphology and structure of the electrospun PTFE/PVDF fibres were investigated through the scanning electron microscope (SEM) (Phenom ProX, Thermo Fisher Scientific) and tunnelling electron microscope (TEM) (HT7700, Hitachi). The chemical composition and structure of the material were analysed using a Fourier transform infrared (FTIR) spectrometer (Nicolet iS5, Thermo Fisher Scientific), and x-ray diffraction analysis (XRD) (D8 Advance, Bruker) was used to analyse the crystalline phase of the PTFE/PVDF electrospun fibre.

2.3. Electromechanical characterisation

The PTFE/PVDF electrospun fibre mat was cut down to 4 cm × 5 cm and then bonded to Cu tape, which works as an electrode. The copper electrodes are fabricated from a single-sided adhesive copper tape, and the fibres are simply attached to the adhesive layer. The other side of the triboelectric test set up used nylon fabric as the triboelectric donor material. This was similarly bonded to a Cu electrode, and the materials were tested with a separation distance of 1.5 cm. A controlled pressure of approximately 0.5 N cm^{-2} (measured using force sensor FSR402) applied at different frequencies (3–9 Hz) using the cyclical compression test system ('tapping rig') shown in figure 2(a). This tested the materials in the vertical contact separation mode (figure 2(b)) resulting in voltage and current pulses as shown in figure 2(c).

As illustrated in figure 8(a), the 4 cm × 5 cm PDVF/PTFE electrospun fibre mat was also assembled alongside the nylon fabric into a folded-over book-shaped triboelectric harvester using a PVC substrate. The book shaped assembly was used to demonstrate the illumination of an LED array and test the ability to charge a capacitor.

The open circuit voltage (V_{oc}) output of the energy harvester was measured using an oscilloscope (MSO7012B, Agilent Technologies) with the 10 MΩ probe resistance. During open circuit voltage measurement, the oscilloscope was connected to the 1 GΩ as a voltage divider circuit due to the large internal impedance of the TENG. The DC power analyser (N6705B, Agilent Technologies) was used to measure the short circuit current (I_{sc}).

3. Results and discussion

3.1. Morphological analysis

Figure 3 show the surface morphologies observed in the SEM of the PTFE/PVDF electrospun fibre at the various PTFE and PVDF ratios. The surface of the 100% PVDF fibre (figure 3(a)) is smooth without any visible bead-like structures. This is the base fibre material used as a benchmark in the study of the effects of the additive PTFE powder. The addition of the PTFE powder to the base PVDF material can be seen to cause increasing fibre surface roughness with increasing amounts of PTFE microparticles. The PTFE/PVDF solution enabled successful electrospinning of the porous fibre mat up to a concentration of 16% PVDF with 4% of the PTFE particles (figure 3(e)). Beyond this, when more than 5% of PTFE was added to the solution, the electrospinning process could not consistently produce PTFE/PVDF fibres producing a combination of fibrous and film like deposits shown in figures 3(f)–(h). This was due to the decreased conductivity of the PTFE/PVDF solution which affects the behaviour of the electrospinning process. The PTFE4/PVDF16 solution yield the 20/80 PTFE/PVDF fibre which were investigated in the TEM, the sample code of the PTFE/PVDF fibre can be found in the table 2. The TEM images in figures 4(a) and (b) indicate the location of PTFE particles in the PVDF fibre demonstrating these have been successfully blended in the starting solution and distributed across the PVDF matrix. The PTFE particle size embedded in PVDF strain was found to be less than 1 μm due to the sonication process before electrospinning preparation.

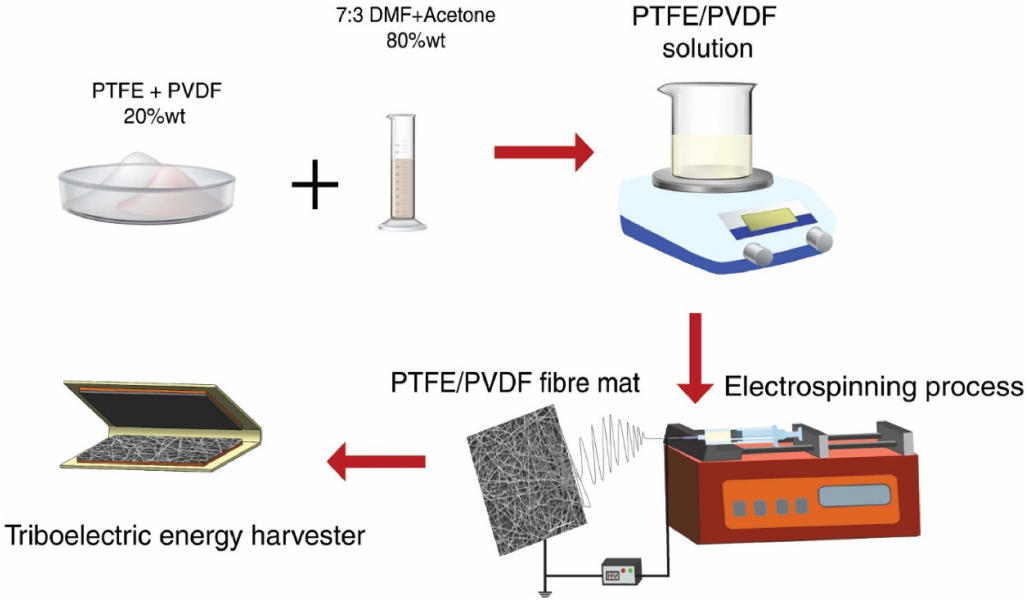

Figure 1. The flow chart describes the PTFE/PVDF electrospun fibre preparation.

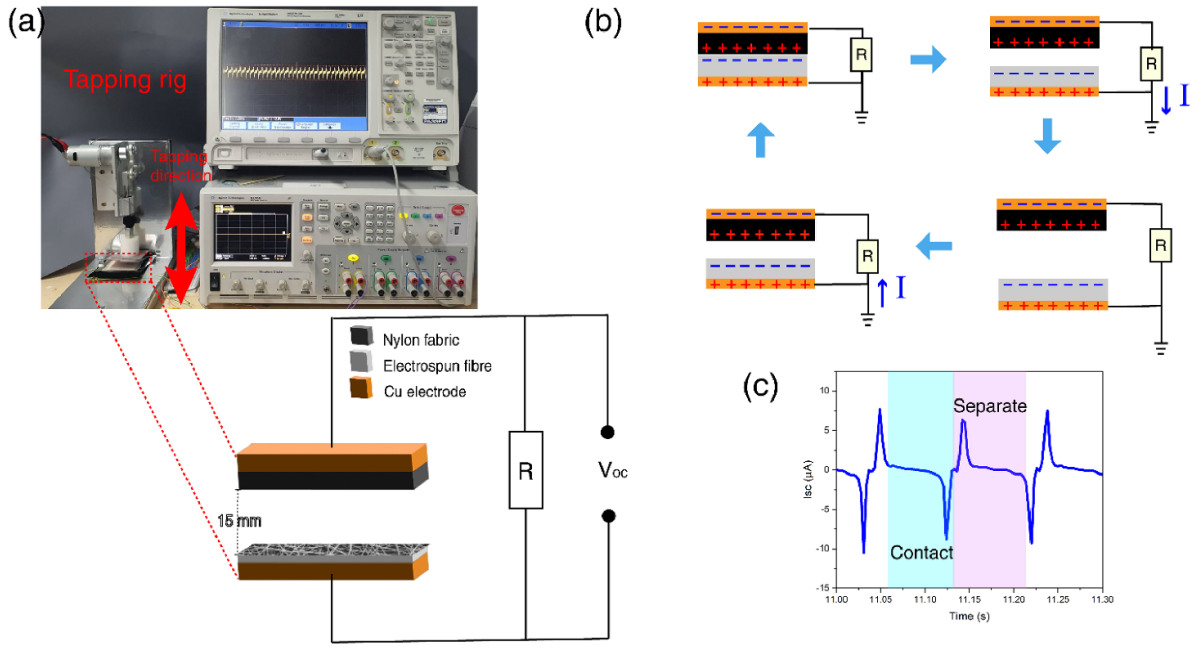

Figure 2. (a) Schematic of PTFE/PVDF triboelectric assembly and photograph of the tapping test rig; (b) working principle in the contact separation mode; (c) example plot of the short circuit current.

3.2. Structural analysis

The FTIR measured chemical composition of PTFE/PVDF electrospun fibres are shown in figure 5(a) alongside the results for the PDVF and PTFE powders. All samples of the PTFE/PVDF electrospun fibres exhibit the characteristic peaks at 840 and 877, representing the β- and C–H wagging in the α-phase of PVDF, respectively. When compared with the results obtained from PVDF powder, which shows peaks at 614, 764, 796, 877, 976, and 1170, it is evident the crystalline piezoelectric β-phase has been effectively induced by the electrospinning process [44, 45]. It is well known that the electrospinning process encourages the β-phase of PVDF due to the strong electric field induced in the polymer solution during whipping of the fibres [44, 46]. Also, the incorporation of PTFE into the electrospun PVDF can be observed at the peak 1170, representing the perturbation of the C=F bond of PTFE and PVDF, as both consist of carbon and fluorine atoms. The characteristics of the PTFE powder spectrum is represented in the peaks 1201 and 1150, which correspond to the asymmetrical and symmetrical CF_2-stretching [47], whereas peaks 642 and 630 represent the C–F deformation [48, 49].

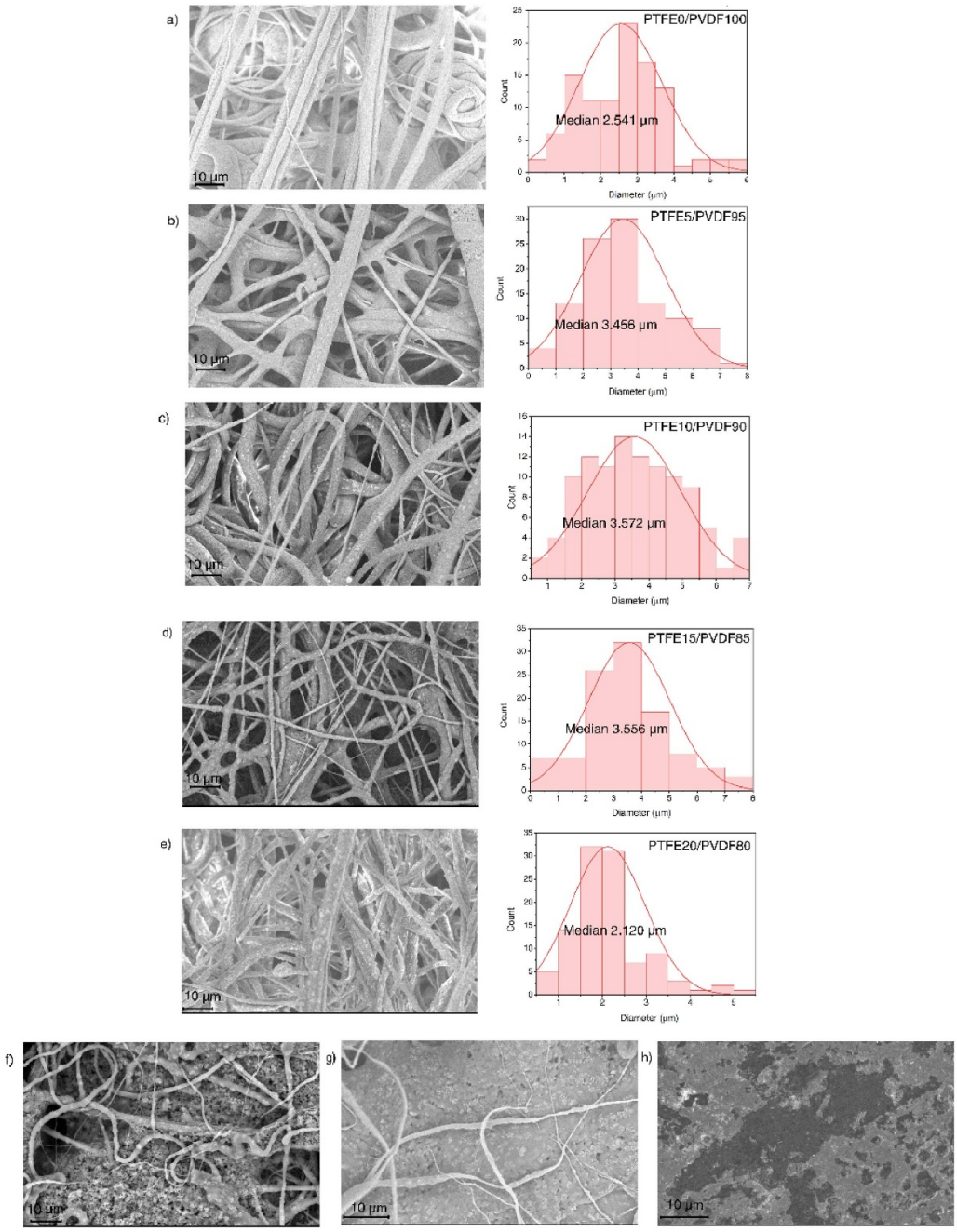

Figure 3. The SEM images (operated at 10 kV) of the single PTFE/PVDF fibre with fibre size distribution curve prepared by different PTFE/PVDF ratios (a) PTFE0/PVDF100, (b) PTFE5/PVDF95, (c) PTFE10/PVDF90, (d) PTFE15/PVDF85, (e) PTFE20/PVDF80, (f) PTFE25/PVDF75, (g) PTFE30/PVDF70 and (h) PTFE35/PVDF65.

The XRD pattern of the PTFE/PVDF electrospun fibre at different percentages of PTFE are shown in figure 5(b). The pure PVDF electrospun fibre exhibits only one strong peak at 20.6° (110/200), representing the β-phase of the PVDF. After introducing PTFE in the PVDF electrospun fibre, the α-phase at a peak of 18.4° (020) occurred and was related to the amount of PTFE in the PVDF fibre. The intensity of the α-phase at a peak of 18.4° (020) becomes stronger as the percentage of PTFE increases. Table 1 shows the crystallinity index (CI) obtained from the XRD results which is calculated by

$$\%\text{Crystallinity} = \frac{S_c}{S_t} \tag{1}$$

where S_c represents the area under the curve at the peak crystalline alpha and beta phases and S_t represent the total area under the plot [50].

This interesting behaviour can be explained by the electric field during the electrospinning process. The β-phase PVDF can be induced by a strong electric field in the electrospinning process. When the PTFE particles are added to the PVDF

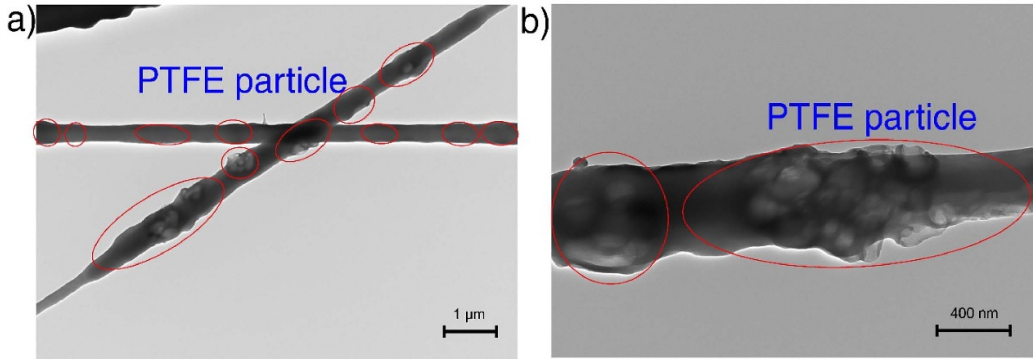

Figure 4. TEM images were measured at acceleration voltage 100 kV, filament voltage 25 kV for a single PTFE20/PVDF80 fibre which was coated on the mesh copper grids at magnification (a) 7000x (b) 25000x.

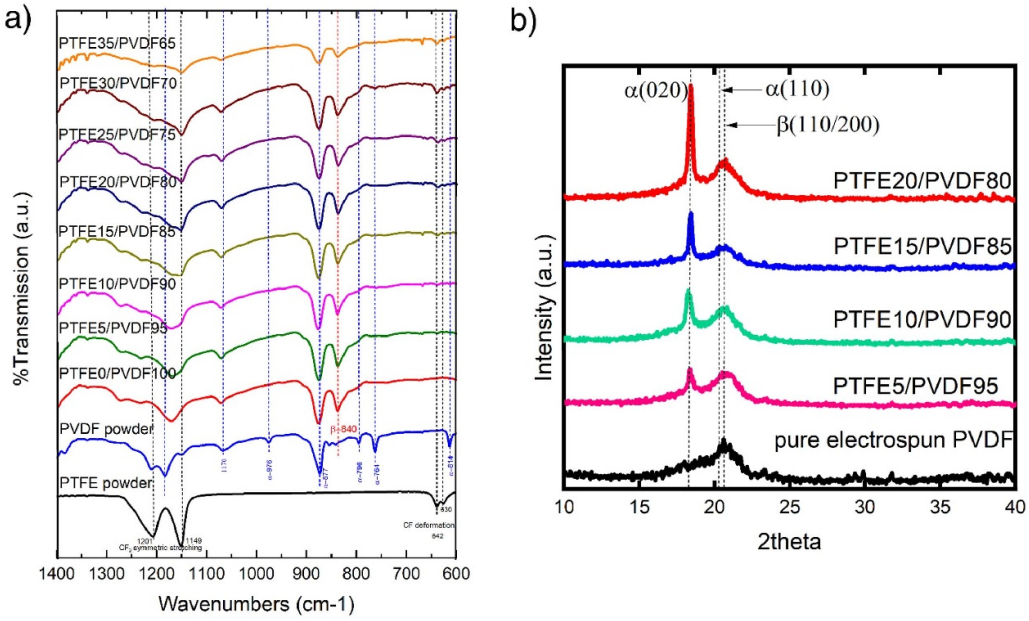

Figure 5. (a) FTIR-ATR spectra of PTFE-PVDF electrospun fibre. The measurements were carried out at room temperature over the range of 600–1400 cm^{-1} (b) XRD spectra of the single PTFE-PVDF electrospun fibre. The analyses were conducted on samples using Cu–Kα_1 radiation 1.5406 Å, 40 kV and 25 mA, Step size 0.5.

Table 1. Crystallinity index obtained from XRD.

	Crystallinity index (%)	
	α-Phase	β-Phase
PTFE0/PVDF100	0	47.50
PTFE5/PVDF95	12.73	29.64
PTFE10/PVDF90	16.09	29.42
PTFE15/PVDF85	18.16	24.63
PTFE20/PVDF80	23.62	20.03

solution, the dielectric properties of the PTFE/PVDF solution increase, resulting in a reduced electric field to induce β-phase. The α-phase requires less energy than the β-phase to form and thus, the β-phase decreases while the α-phase increases as shown in table 1.

In summary, both the FTIR and XRD spectra results indicate that the PTFE/PVDF electrospun fibres have a mix of α- and β-phase PVDF. The amount of the β-Phase decreases, and the α-phase increases with an increase in percentage of PTFE. In addition, the electromechanical performance of the PTFE/PVDF presented in section 3.3 is not related to the piezoelectric phase of the PVDF. It confirms that the β-phase of PVDF (exhibiting piezoelectric properties) is not the key to high energy harvesting performance in the hybrid piezo-triboelectric-based design. The relationship between the number of fluorine atoms which increases the negative charge and the surface morphology of the PTFE/PVDF fibre was responsible for the triboelectric effect. When more fluorine atoms at higher PTFE percentages are added, the texture of the fibre becomes non-porous due to unsuitable electrospinning conditions. This results in a change in surface morphology that leads to a decrease in the electromechanical performance. This relationship is supported by surface potential measurements taken using the static fieldmeter SIMCO-FX003. These measurements showed wide variations depending upon location on

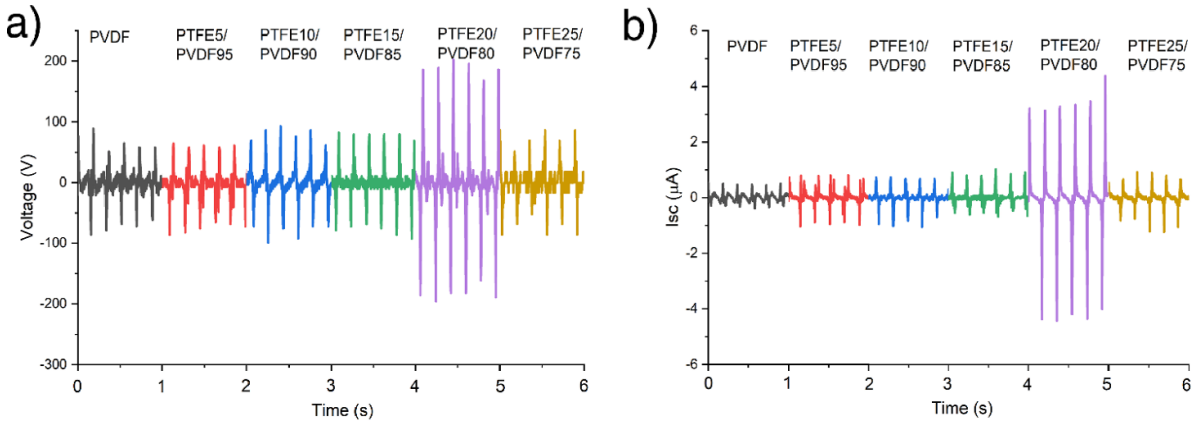

Figure 6. (a) open circuit voltage was tested across a 1 GΩ load resistor and (b) short circuit current of the PTFE/PVDF electrospun fibre prepared at different concentrations.

the fibre mat and the corresponding thickness at that point, but the average potential of PVDF and PTFE20/PVDF80 were 1.1 and 1.8 kV, respectively.

3.3. Electromechanical study

The energy harvesting performance was initially tested with the tapping rig in order to explore the optimum PTFE concentration. The test was performed at 6 Hz using the contact separation triboelectric mode (figures 2(a) and (b)). The V_{oc} and I_{sc} of each sample prepared from different concentrations were read after tapping for approximately 3 min to ensure that the tapping rate and the signal output were consistent. When the surfaces make contact, there is an electron transfer from the positively charged nylon to the negatively charged electrospun PTFE/PVDF. This leads to the nylon surface gaining a positive charge and the electrospun PTFE/PVDF surface developing a negative charge. When the surfaces are separated, an induced potential difference between the electrodes arises, leading to the development of opposite transferred charges on the electrodes through electrostatic induction. Consequently, an electric charge will transfer from the bottom electrode to the top electrode via an external load in order to balance the potential difference until it reaches a state of equilibrium. As the surfaces approach each other, the potential difference caused by tribo-charging will gradually decrease until it reaches zero. The charges that were transferred are now moving in the opposite direction, from the top to the bottom electrode.

The open circuit voltage (V_{oc}) and short circuit current (I_{sc}) output measured at a 6 Hz tapping rate are shown in figures 6(a) and (b) respectively. The V_{oc} and I_{sc} obtained from pure PVDF are slightly less than those obtained from other samples that include PTFE particles. The output from PTFE5/PVDF95, PTFE10/PVDF90 and PTFE15/PVDF85 were similar which relates to the similar fibre size which results in the PTFE particles being similarly distributed within the fibres. For the PTFE20/PVDF80 sample, as shown in figure 3(e), the fibre size is smaller and, combined with the higher percentage of PTFE particles, there is a greater concentration of PTFE at the surface of the fibres. This increases the triboelectric effect due to the superior triboelectric properties of the PTFE. When the PTFE particles exceed 20% (samples PTFE25/PVDF75, PTFE30/PVDF70, and PTFE35/PVDF65) the electrospinning process could not correctly form the fibres, resulting in poor mixing of PTFE particles and PVDF binder and thus the output is reduced in comparison with the PTFE20/PVDF80 (as seen in figures 6(a) and (b)). It was found that the peak-to-peak V_{oc} shows a similar output for pure PVDF and up to PTFE15/PVDF85. The peak-to-peak V_{oc} shows a sharp increase to 390 V for the PTFE20/PVDF80 fibres. The results for the peak-to-peak I_{sc} follow a similar pattern with a maximum peak I_{sc} of 8 μA occurring with the PTFE20/PVDF80. The PTFE20/PVDF80 fibre mat made from the 4% PTFE and 16% PVDF solution gives the highest electrical output and was used in the subsequent analysis to investigate the effectiveness of the contact separation mode triboelectric energy harvesting using the electrospun fibres.

The open circuit voltage (V_{oc}) output and short circuit current (I_{sc}) of the PTFE20/PVDF80 fibre mat were tested at different load resistance (1 kΩ–6 GΩ), as shown in figure 7(a). The calculated peak power ($P = \frac{V_p{}^2}{R}$) and the power density ($P = \frac{V_p{}^2}{RA}$) from the test are plotted in figure 7(b). The highest power and power density were obtained at an optimal load resistance of 10 MΩ and were found to be 7 mW and 348.5 mW m^{-2}, respectively.

The contact-separation mode TENG works with a connected resistor R for this cyclical testing using the tapping rig. The top electrode moves up and down with the separation distance, $x(t)$, from the fixed bottom triboelectric material. According to Ohm's law

$$V(t) = RI(t) = R\frac{\mathrm{d}Q(t)}{\mathrm{d}t} \tag{2}$$

V is the voltage output, Q is the amount of transferred charge between the two electrodes, I is the current output, and R is the load resistance; the V_{oc} and I_{sc} depend on the frequency of cyclical moving on both sides of triboelectric materials as a sinusoidal function that can be described by

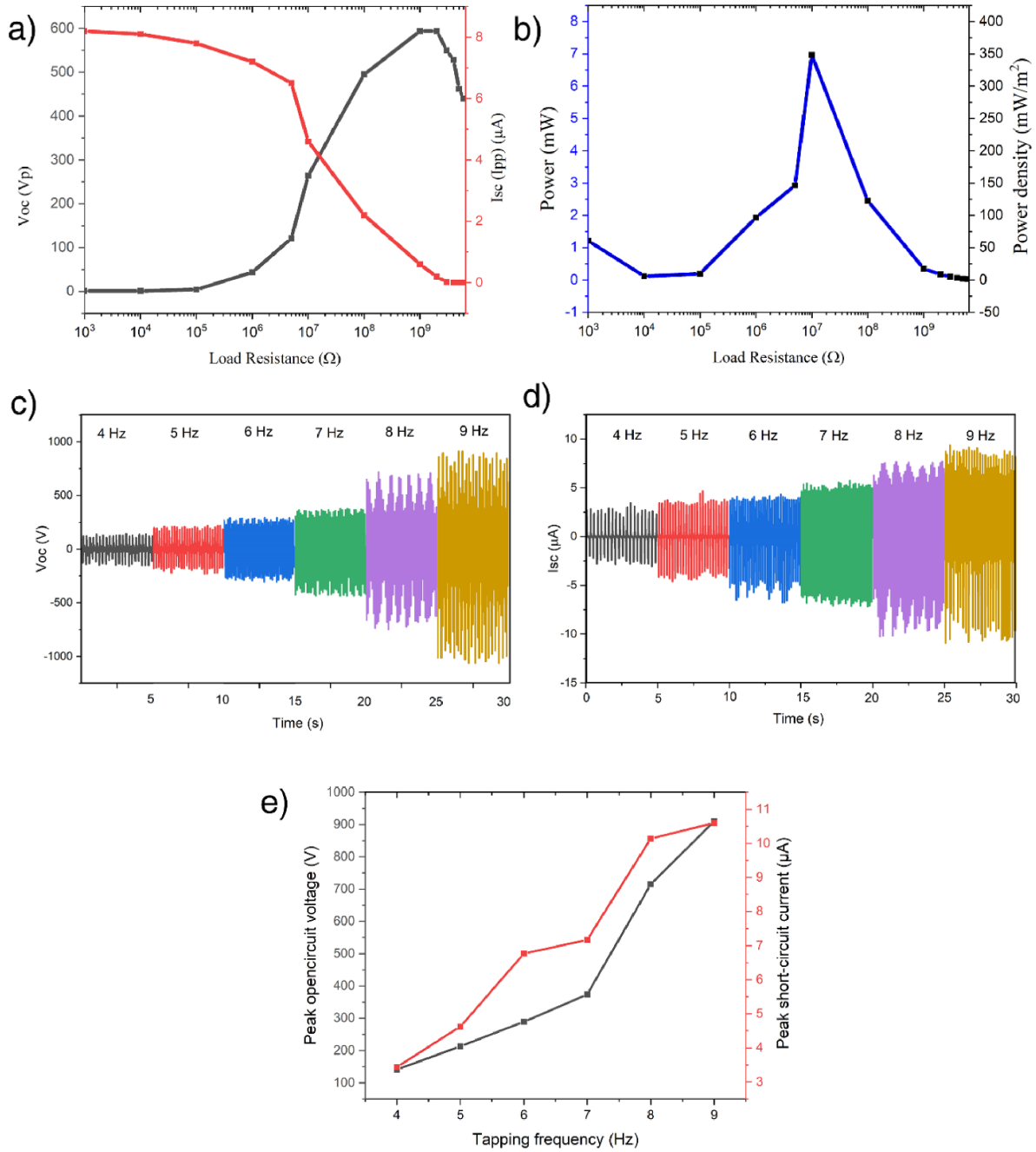

Figure 7. (a) peak open circuit voltage (V_{oc}) and peak to peak short circuit current (I_{sc}) versus load resistance; (b) calculated power and power density of the PTFE4/PVDF16 versus load resistances; (c) V_{oc} and (d) I_{sc} of PTFE4/PVDF16 at different tapping frequencies; (e) peak values of V_{oc} and I_{sc} as a function of tapping frequency.

$x(t) = A\sin(\omega t + \theta)$, where t, A, ω and θ are the time, amplitude, angular velocity and initial phase angle of the cyclical motion, respectively [51, 52].

The V_{oc} and I_{sc} obtained when testing at tapping frequencies of 4–9 Hz are shown in figures 7(c) and (d), peak V_{oc} and I_{sc} versus tapping frequency is plotted in figure 7(e). As expected, the increased tapping frequency resulted in an increase of the V_{oc} and I_{sc}. When increasing the tapping frequency, the top layer contacts and separates the bottom layer quicker, resulting in the charge transfer reaching the equilibrium quicker through the external load. When the charge transfer reaches equilibrium, the output should reach the saturated point and then plateau, as found in the literature [53, 54]. However, the tapping rig used in this work has limitations in testing; thus, the results could not show the saturating point. Table 2 summarizes the results obtained for all samples.

To demonstrate the practical utilisation of the PTFE/PVDF fibre, the book-shaped PVC substrate was assembled with the PTFE20/PVDF80 and the nylon fabric and connected to a full bridge rectifier to convert the AC output to DC to enable the energy to be stored on a capacitor as shown in figure 8(a). This experiment provides an accurate practical assessment of

Table 2. Summary of the electromechanical characteristics of the sample.

Code	Solution mixing condition	Percentage of polymer in fibre	Tapping frequency (Hz)	V_{oc} (peak to peak) (V)	I_{sc}(peak to peak) (μA)
PVDF	PTFE0/PVDF20	PVDF 100%	6	130	1.23
PTFE5/PVDF95	PTFE1%/PVDF19%	PTFE 5%, PVDF95%	6	136	1.63
PTFE10/PVDF90	PTFE2%/PVDF18%	PTFE10%, PVDF90%	6	167	2.45
PTFE15/PVDF85	PTFE3%/PVDF17%	PTFE15%, PVDF85%	6	154	3.11
PTFE20/PVDF80	PTFE4%/PVDF16%	PTFE20%, PVDF80%	6	555	9.04
PTFE25/PVDF75	PTFE5%/PVDF15%	PTFE25%, PVDF75%	6	171	2.10
PTFE20/PVDF80	PTFE4%/PVDF16%	PTFE20%, PVDF80%	4	277	3.95
			5	429	7.68
			6	555	9.04
			7	766	12.24
			8	1422	17.36
			9	1889	19.72

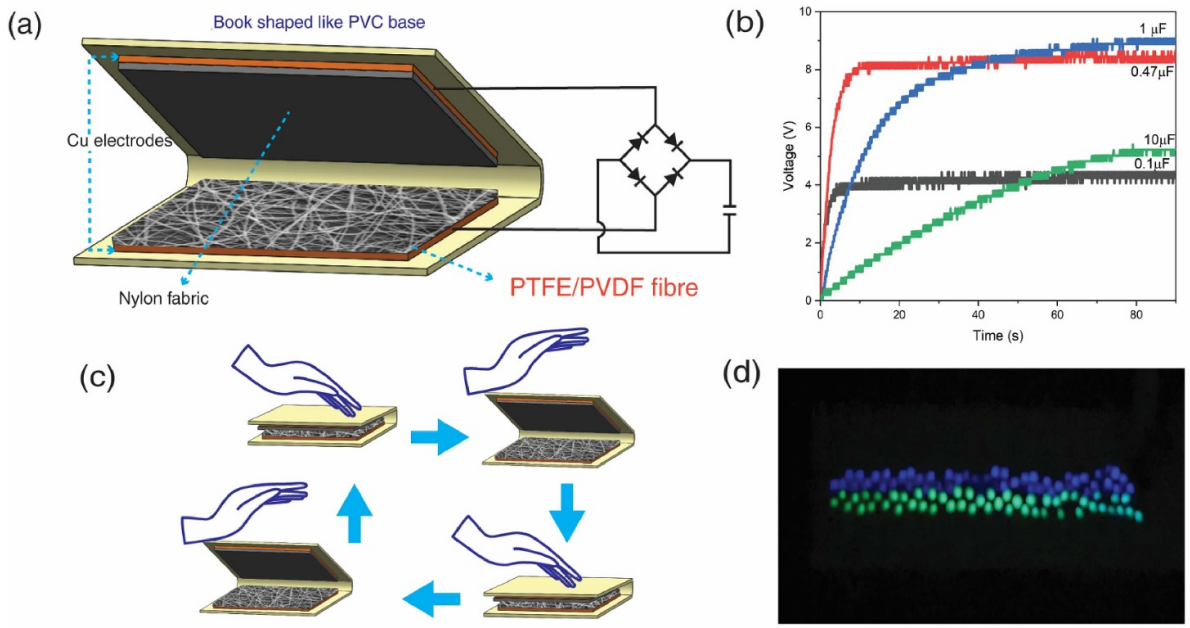

Figure 8. (a) Schematic of the book-shaped triboelectric energy harvester used to charge the capacitors ; (b) the voltage across 0.1, 0.47, 1, and 10 μF capacitors, when charged by the book shaped energy harvester at 6 Hz over a 90 s period; (c) schematic of the hand tapping test during the testing of the 100 LED lights experiment; (d) the 100 LED lights illuminated via hand tapping of the book shaped PTFE/PVDF energy harvester.

the energy that can be harvested and delivered to the energy storage device and includes the losses that occur in the conditioning circuit. The capacitor charging test was performed using the tapping rig with a frequency of 6 Hz with capacitors of 0.1, 0.47, 1, and 10 μF. The calculated energy from charging obtained from $U = \frac{1}{2} CV^2$ was found at the capacitor 0.1, 0.47, 1, and 10 μF is 1.0, 16.7, 41.2 and 136.8 μJ, respectively. The book-shaped TENG was further tested by illuminating an LED array using manual tapping method, as illustrated in figure 8(c). It was found that hand tapping could illuminate 100 LEDs, as shown in figure 8(d). The blue and green LEDs used in this work require at least 3.4 V in order to light one LED bulb. In this case, it can be assumed that the hand tapping TENGs prepared using PTFE/PVDF fibre with a frequency of approximately 6 Hz can generate more than 340 V in order to illuminate 100 LED light bulbs. The illuminated LED bulbs can be seen in the supporting data S1.

To demonstrate the potential energy harvesting output in a practical energy harvesting application, the electropun fibre mat was assembled into a modified shoe insole to harvest energy during walking and running. The insole was modified to include four cut-out sections each 2 cm $\times$ 2 cm placed next to each other resulting in an active area of 16 cm^2 located at the heal of the foot. A rib of insole was left between these sections to ensure the insole remained comfortable to use and to make the active sections imperceptible to the user (see the schematic of insole in figure 9(a)). The harvester operates in the contact separation mode with the electrospun fibre mat making contact with the nylon during the initial contact and loading phases associated with the foot being placed on the

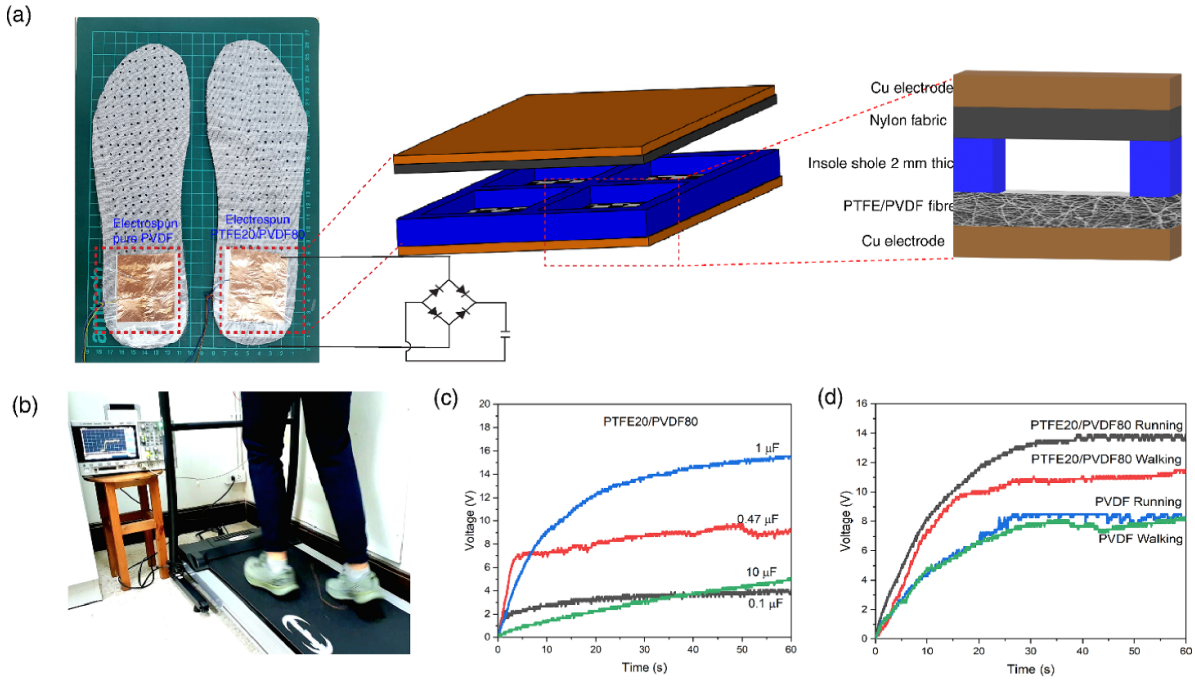

Figure 9. The triboelectric insole for a demonstration of human gait energy harvesting (a) the photo and schematic of the shoe insole used in this study (b) the photo when charging the capacitor when running on the treadmill (c) the voltage across the 1 μF capacitor, when charged by running on the PTFE20/PVDF80 insole over a 60 s period (d) the comparison of the voltage across the 1 μF capacitor, when running and walking on PTFE20/PVDF80 and PVDF insole over a 60 s period.

ground during the gait cycle and separating as the heal lifts off during the terminal stance and pressing phases. The harvester was realised from 100% electrospun PVDF fibres which was placed on the left foot insole, and from PTFE20/PVDF80 electrospun fibre which was used in the right insole (as shown in figure 9(a)) enabling a comparison of the PVDF and electrospun PTFE/PVDF fibres. The insole was placed inside an otherwise normal pair of running shoes and connected to the full bridge rectifier circuit consisting of 1N4007 diodes to charge the capacitors. Figure 9(c) shows the voltage across the 0.1, 0.47, 1.0 and 10 μF capacitors that was measured during running on treadmill, as can be seen in the supporting data S2. The calculated energy obtained from running using the formula $U = \frac{1}{2}CV^2$ at capacitors 0.1, 0.47, 1, and 10 μF was found to be 0.7, 15.8, 100.8 and 105.8 μJ, respectively. Figure 9(d) shows the comparison of the voltage across the 1 μF capacitor between the insole made from the pure PVDF and PTFE20/PVDF80 when charging by walking and running. The calculated energy obtained from the PVDF insole from running and walking was 25.9 and 27.4 μJ, respectively. While the calculated energy obtained from the PTFE20/PVDF80 insole from running and walking was 69.6 and 100.8 μJ, respectively. The energy obtained from the insole made from PTFE20/PVDF80 was shown to be approximately 3 times greater when walking and 4 times greater when running than the PVDF insole.

4. Conclusion

It was possible to effectively prepare a flexible PTFE fibre utilising a one-step electrospinning process with a PVDF solution as a precursor. An examination was conducted on the energy harvesting performance of a triboelectric assembly operating in a vertical contact separation mode with electrospun fibres with different percentages of PTFE as the negative materials and nylon as the triboelectric positive material. The electrospun fibres created a nonwoven textile mat with promising negative surface potential with the optimum percentage being 20% PTFE loading in the PVDF matrix. This percentage of PTFE in the electrospun fibre enhanced the voltage and current output by 4 and 7 times, respectively but it, was found that the maximum power density was 348.5 mW m^{-2} at a 10 MΩ resistance. Additionally, the application of the electrospun fibres was further demonstrated in book-shaped and shoe insole based triboelectric harvesters operating in the contact separation mode. The book shaped harvester assembled with the PVDF energy harvester can successfully charge an energy storage capacitor using a full bridge rectifier circuit pointing the way towards energy harvesting powered systems. Electrospinning is a straightforward process for fabricating fibres that can be directly used in a non-woven fibre mat that is entirely compatible with textiles being soft, breathable, and conformable. Fibres could also be used to fabricate triboelectric PTFE/PVDF threads that could be combined within a woven or knitted textile. The improvements in electrical output from the fibres with PTFE certainly merit further investigation in practical energy harvesting applications. The influence of the PTFE particles on the surface roughness of the fibres has not been quantified in this study. This surface roughness can affect the output of the TENG and therefore this will be studied in future work using an atomic force microscope.

Data availability statement

All data that support the findings of this study are included within the article (and any supplementary files).

Acknowledgments

Pattarinee White expresses her gratitude to the Royal Thai Government Scholarship for kindly providing support for her research. Under the Chairs in Emerging Technologies Scheme, the U.K. Royal Academy of Engineering provided support for Stephen Beeby's study.

Conflict of interest

The authors declare no conflict of interest.

CRediT authorship contribution statement

Pattarinee White: Review, Investigation, Writing—original draft, Validation, Methodology. **Piyapong Pankaew**: Investigation, Formal analysis, Resources. **Dmitry Bavykin**: Supervision, Resources, Formal analysis. **Mohamed Moshrefi-Torbati**: Supervision, Resources, Conceptualization, **Stephen Beeby**: Supervision, Conceptualization, Resources, Writing—review & editing

Funding

This research received no external funding.

ORCID iDs

Pattarinee White https://orcid.org/0000-0001-6341-6378
Piyapong Pankaew https://orcid.org/0000-0001-5099-403X
M Moshrefi-Torbati https://orcid.org/0000-0003-3112-6354
Stephen Beeby https://orcid.org/0000-0002-0800-1759

References

[1] Research G V 2023 Wearable technology market share & trends report (available at: www.grandviewresearch.com/industry-analysis/wearable-technology-market)
[2] Melchor-Martínez E M, Macias-Garbett R, Malacara-Becerra A, Iqbal H M N, Sosa-Hernández J E and Parra-Saldívar R 2021 Environmental impact of emerging contaminants from battery waste: a mini review *Case Stud. Chem. Environ. Eng.* **3** 100104
[3] Islam M T, Huda N, Baumber A, Hossain R and Sahajwalla V 2022 Waste battery disposal and recycling behavior: a study on the Australian perspective *Environ. Sci. Pollut. Res.* **29** 58980–9001
[4] Komolafe A, Zaghari B, Torah R, Weddell A S, Khanbareh H and Tsikriteas Z M 2021 E-textile technology review-from materials to application *IEEE Access* **9** 97152–79
[5] Zeyrek Ongun M *et al* 2020 Aligned PVDF-TrFE nanofibers with high-density PVDF nanofibers and PVDF core-shell structures for endovascular pressure sensing *J. Mater. Sci., Mater. Electron.* **31** 188–95
[6] Kim S, Towfeeq I, Dong Y, Gorman S, Rao A and Koley G 2018 P(VDF-TrFE) film on PDMS substrate for energy harvesting applications *Appl. Sci.* **8** 213
[7] Ghosh S K, Sinha T K, Xie M, Bowen C R, Garain S and Mahanty B 2021 Temperature-pressure hybrid sensing all-organic stretchable energy harvester *ACS Appl. Electron. Mater.* **3** 248–59
[8] Halim M A, Cho H, Salauddin M and Park J Y 2016 A miniaturized electromagnetic vibration energy harvester using flux-guided magnet stacks for human-body-induced motion *Sens. Actuators* A **249** 23–31
[9] Shi J, Yong S and Beeby S 2018 An easy to assemble ferroelectret for human body energy harvesting *Smart Mater. Struct.* **27** 084005
[10] Wan H, Cao Y, Lo L W, Zhao J, Sepúlveda N and Wang C 2020 Flexible carbon nanotube synaptic transistor for neurological electronic skin applications *ACS Nano* **14** 10402–12
[11] Busolo T, Ura D P, Kim S K, Marzec M M, Bernasik A and Stachewicz U 2019 Surface potential tailoring of PMMA fibers by electrospinning for enhanced triboelectric performance *Nano Energy* **57** 500–6
[12] Paosangthong W, Wagih M, Torah R and Beeby S 2019 Textile-based triboelectric nanogenerator with alternating positive and negative freestanding grating structure *Nano Energy* **66** 104148
[13] Paosangthong W, Wagih M, Torah R and Beeby S 2022 Textile-based triboelectric nanogenerator with alternating positive and negative freestanding woven structure for harvesting sliding energy in all directions *Nano Energy* **92** 106739
[14] Due J, Munk-Nielsen S and Nielsen R 2010 Energy harvesting with di-electro active polymers *IET Conf. Publ* vol 2010 (563 CP)
[15] McKay T G, Rosset S, Anderson I A and Shea H 2013 An electroactive polymer energy harvester for wireless sensor networks *J. Phys.: Conf. Ser.* **476** 0–5
[16] Elbarmaki J, EL Jouad M, Belhora F and Hajjaji A 2022 Wave energy harvesting using Silicone as Electro-active Polymers *Mater. Today* **66** 22–25
[17] Pan S and Zhang Z 2019 Fundamental theories and basic principles of triboelectric effect: a review *Friction* **7** 2–17
[18] Munirathinam P, Anna Mathew A, Shanmugasundaram V, Vivekananthan V, Purusothaman Y, Kim S J and Chandrasekhar A 2023 A comprehensive review on triboelectric nanogenerators based on real-time applications in energy harvesting and self-powered sensing *Mater. Sci. Eng.* B **297** 116762
[19] Fan F R, Tian Z Q and Lin Wang Z 2012 Flexible triboelectric generator *Nano Energy* **1** 328–34
[20] Lai Y C, Hsiao Y C, Wu H M and Wang Z L 2019 Waterproof fabric-based multifunctional triboelectric nanogenerator for universally harvesting energy from raindrops, wind, and human motions and as self-powered sensors *Adv. Sci.* **6** 1801883
[21] He T, Shi Q, Wang H, Wen F, Chen T, Ouyang J and Lee C 2019 Beyond energy harvesting—multi-functional triboelectric nanosensors on a textile *Nano Energy* **57** 338–52
[22] He M, Du W, Feng Y, Li S, Wang W, Zhang X, Yu A, Wan L and Zhai J 2021 Flexible and stretchable triboelectric nanogenerator fabric for biomechanical energy harvesting and self-powered dual-mode human motion monitoring *Nano Energy* **86** 106058
[23] Lama J, Yau A, Chen G, Sivakumar A, Zhao X and Chen J 2021 Textile triboelectric nanogenerators for self-powered biomonitoring *J. Mater. Chem.* A **9** 19149–78

[24] Šutka A, Lapčinskis L, He D, Kim H, Berry J D, Bai J, Knite M, Ellis A V, Jeong C K and Sherrell P C 2023 Engineering polymer interfaces: a review toward controlling triboelectric surface charge *Adv. Mater. Interfaces* **10** 2300323

[25] Lee K Y, Kim S K, Lee J-H, Seol D, Gupta M K, Kim Y and Kim S-W 2016 Controllable charge transfer by ferroelectric polarization mediated triboelectricity *Adv. Funct. Mater.* **26** 3067–73

[26] Šutka A, Malnieks K, Linarts A, Timusk M, Jurķans V, Gorņevs I, Blūms J, Bērziņa A, Joost U and Knite M 2018 Inversely polarised ferroelectric polymer contact electrodes for triboelectric-like generators from identical materials *Energy Environ. Sci.* **11** 1437–43

[27] Lee J P, Lee J W and Baik J M 2018 The progress of PVDF as a functional material for triboelectric nanogenerators and self-powered sensors *Micromachines* **9** 30–33

[28] Garcia C, Trendafilova I, Guzman de Villoria R and Sanchez Del Rio J 2018 Self-powered pressure sensor based on the triboelectric effect and its analysis using dynamic mechanical analysis *Nano Energy* **50** 401–9

[29] Garcia C and Trendafilova I 2019 Real-time diagnosis of small energy impacts using a triboelectric nanosensor *Sens. Actuators* A **291** 196–203

[30] Garcia C, Trendafilova I and Sanchez Del Rio J 2019 Detection and measurement of impacts in composite structures using a self-powered triboelectric sensor *Nano Energy* **56** 443–53

[31] Hao Y, Bin Y, Tao H, Cheng W, Hongzhi W and Meifang Z 2015 Preparation and optimization of Polyvinylidene fluoride (PVDF) triboelectric nanogenerator via electrospinning *IEEE-NANO 2015–15th Int. Conf. Nanotechnology* vol 1 pp 1485–8

[32] Guo Y, Zhang H, Zhong Y, Shi S, Wang Z, Wang P and Zhao Y 2023 Triboelectric nanogenerator-based near-field electrospinning system for optimizing PVDF fibers with high piezoelectric performance *ACS Appl. Mater. Interfaces* **15** 5242–52

[33] Shaikh M O, Huang Y B, Wang C C and Chuang C H 2019 Wearable woven triboelectric nanogenerator utilizing electrospun PVDF nanofibers for mechanical energy harvesting *Micromachines* **10** 438

[34] Tofel P, Částková K, Říha D, Sobola D, Papež N, Kaštyl J, Ţălu Ş and Hadaš Z 2022 Triboelectric response of electrospun stratified PVDF and PA structures *Nanomaterials* **12** 349

[35] Al-Attabi R *et al* 2023 Durable and comfortable electrospun nanofiber membranes for face mask applications *Sep. Purif. Technol.* **322** 124370

[36] Lee J W, Ye B U and Baik J M 2017 Research update: recent progress in the development of effective dielectrics for high-output triboelectric nanogenerator *APL Mater.* **5** 073802

[37] Schröder S, Strunskus T, Rehders S, Gleason K K and Faupel F 2019 Tunable polytetrafluoroethylene electret films with extraordinary charge stability synthesized by initiated chemical vapor deposition for organic electronics applications *Sci. Rep.* **9** 1–7

[38] Kang D, Lee H Y, Hwang J-H, Jeon S, Kim D, Kim S M and Kim S-W 2022 Deformation-contributed negative triboelectric property of polytetrafluoroethylene: a density functional theory calculation *Nano Energy* **100** 107531

[39] Lin S, Cheng Y, Mo X, Chen S, Xu Z, Zhou B, Zhou H, Hu B and Zhou J 2019 Electrospun polytetrafluoroethylene nanofibrous membrane for high-performance self-powered sensors *Nanoscale Res. Lett.* **14** 251

[40] Xiong J, Huo P and Ko F K 2009 Fabrication of ultrafine fibrous polytetrafluoroethylene porous membranes by electrospinning *J. Mater. Res.* **24** 2755–61

[41] Zhao P, Soin N, Prashanthi K, Chen J, Dong S and Zhou E 2018 Emulsion electrospinning of polytetrafluoroethylene (PTFE) nanofibrous membranes for high-performance triboelectric nanogenerators *ACS Appl. Mater. Interfaces* **10** 5880–91

[42] White P, Bavykin D, Moshrefi-Torbati M and Beeby S 2023 The energy harvesting performance of a flexible triboelectric-based electrospun PTFE/PVDF fibre *Eng. Proc.* **30** 3–7

[43] Windey R, AhmadvashAghbash S, Soete J, Swolfs Y and Wevers M 2023 Ultrasonication optimisation and microstructural characterisation for 3D nanoparticle dispersion in thermoplastic and thermosetting polymers *Composites* B **264** 110920

[44] Medeiros K A R, Rangel E Q, Sant'Anna A R, Louzada D R, Barbosa C R H and D'Almeida J R M 2018 Evaluation of the electromechanical behavior of polyvinylidene fluoride used as a component of risers in the offshore oil industry *Oil Gas Sci. Technol.* **73** 48

[45] Bairagi S, Khandelwal G, Karagiorgis X, Gokhool S, Kumar C, Min G and Mulvihill D M 2022 High-performance triboelectric nanogenerators based on commercial textiles: electrospun nylon 66 nanofibers on silk and pvdf on polyester *ACS Appl. Mater. Interfaces* **14** 44591–603

[46] Lee B-S, Park B, Yang H S, Han J W, Choong C and Bae J 2014 Effects of substrate on piezoelectricity of electrospun poly(vinylidene fluoride)-nanofiber-based energy generators *ACS Appl. Mater. Interfaces* **6** 3520–7

[47] Piwowarczyk J, Jedrzejewski R, Moszy´nski D, Kwiatkowski K, Niemczyk A and Baranowska J 2019 XPS and FTIR studies of polytetrafluoroethylene thin films obtained by physical methods *Polymers* **11** 1–13

[48] Mihály J, Sterkel S, Ortner H M, Kocsis L, Hajba L and Furdyga É 2006 FTIR and FT-Raman spectroscopic study on polymer based high pressure digestion vessels *Croat. Chem. Acta* **79** 497–501 (available at: https://hrcak.srce.hr/file/8817)

[49] Barylski A, Aniołek K, Swinarew A S, Kaptacz S, Gabor J, Waśkiewicz Z and Stanula A 2020 Novel organic material induced by electron beam irradiation for medical application *Polymers* **12** 1–11

[50] Rotaru R, Savin M, Tudorachi N, Peptu C and Samoila P 2018 Ferromagnetic iron oxide–cellulose nanocomposites prepared by ultrasonication polymer chemistry nanocomposites prepared by ultrasonication *Polym. Chem.* **9** 860–8

[51] Yang B, Zeng W, Peng Z H, Liu S R, Chen K and Tao X M 2016 A fully verified theoretical analysis of contact-mode triboelectric nanogenerators as a wearable power source *Adv. Energy Mater.* **6** 1–8

[52] Zhao H, Wang H, Yu H, Xu Q, Li X, Guo J, Shao J, Wang Z L, Xu M and Ding W 2024 Theoretical modeling of contact-separation mode triboelectric nanogenerators from initial charge distribution *Energy Environ. Sci.* **17** 2228–47

[53] Rana S M S, Rahman M T, Salauddin M, Sharma S, Maharjan P, Bhatta T, Cho H, Park C and Park J Y 2021 Electrospun PVDF-TrFE/MXene nanofiber mat-based triboelectric nanogenerator for smart home appliances *ACS Appl. Mater. Interfaces* **13** 4955–67

[54] Xiong J, Cui P, Chen X, Wang J, Parida K, Lin M-F and Lee P S 2018 Skin-touch-actuated textile-based triboelectric nanogenerator with black phosphorus for durable biomechanical energy harvesting *Nat. Commun.* **9** 1–9